Journal of Molecular Structure 1154 (2018) 301–318

Contents lists available at ScienceDirect

Journal of Molecular Structure

journal homepage: http://www.elsevier.com/locate/molstruc

The structural, electronic and spectroscopic properties of 4FPBAPE molecule: Experimental and theoretical study

Emine Tanış [a, *], Emine Babur Sas [b], Mustafa Kurban [b], Mustafa Kurt [c]

[a] Kaman Vocational Schools, Ahi Evran University, Kırşehir, Turkey
[b] Department of Electronics and Automation, Ahi Evran University, Kırşehir, Turkey
[c] Department of Physics, Ahi Evran University, Kırşehir, Turkey

ARTICLE INFO

Article history:
Received 11 September 2017
Received in revised form
15 October 2017
Accepted 16 October 2017
Available online 19 October 2017

Keywords:
4FPBAPE
DFT
Fourier transform infrared spectroscopy
Dispersive Raman spectra
Nuclear magnetic resonance
Dimethyl sulfoxide

ABSTRACT

The experimental and theoretical study of 4-Formyl Phenyl Boronic Acid Pinacol Ester (4FPBAPE) molecule were performed in this work. ^{1}H, ^{13}C NMR and UV–Vis spectra were tested in dimethyl sulfoxide (DMSO). The structural, spectroscopic properties and energies of 4FPBAPE were obtained for two potential conformers from density functional theory (DFT) with B3LYP/6-311G (d, p) and CAM-B3LYP/6-311G (d, p) basis sets. The optimal geometry of those structures was obtained according to the position of oxygen atom upon determining the scan coordinates for each conformation. The most stable conformer was found as the A_2 form. The fundamental vibrations were determined based on optimized structure in terms of total energy distribution. Electronic properties such as oscillator strength, wavelength, excitation energy, HOMO, LUMO and molecular electrostatic potential and structural properties such as radial distribution functions (RDF) and probability density depending on coordination number are presented. Theoretical results of 4-FPBAPE spectra were found to be compatible with observed spectra.

1. Introduction

The compounds of Boronic acid and its derivatives have drawn remarkable interest in recent years. This growing interest in Boronic acids ensues from their classification as powerful Lewis acids [1]. The open-shell of Boron allows the change in hybridization of Boron atom from sp^2 trigonal to sp^3 tetrahedral in the presence of Lewis bases [1–3]. That is why Boronic acids and derivatives are applied in a great deal of fields, particularly in organic chemistry and medicine. In materials science, for example, Boronic acid pinacol esters are utilized as starting materials in organic synthesis for Suzuki-Miyaura chemistry [4]. In medicine, ^{10}B isotope can be irradiated with neutrons to diffuse short range α particles in tissue [5–14] and Boron-based compounds enable the application of Boron-10 neutron capture therapy (BNCT) in tumor sites [15]. Boronic acids have been added into amino and nucleo acids as antitumor antiviral substances [16]. Phenylboronic acid derivatives have been synthesized as antimetabolite against cancer [17–19]. Likewise, formylphenylboronic acids find application in agrochemical and pharmaceutical industries as effective enzyme stabilizers, inhibitors, and bactericides [3].

There are a number of studies on phenylboronic acids and derivatives. For example, Cyrański et al. [20] have searched the structural properties of phenylboronic acid and its dimer. Horton et al. [21] have researched the crystal structure of pentafluorophenylboronic acid. Shimpi et al. [22] have examined the crystal structures of 4-chloro- and 4-bromophenyboronic acids and hydrates of 2- and 4-iodophenylboronic acid. Rodriguez-Cuamatzi et al. [23] and Bradley et al. [24] have investigated the crystal structures of 2,4-difluorophenylboronic acid, 3-fluorophenylboronic acid and (2,6-difluorophenyl) dihydroxyborane, respectively. Faniran [25] has studied the infrared spectra of phenylboronic acid and diphenyl phenylboronate molecules. Erdogdu et al. [26] carried out 2-fluorophenylboronic acid using theoretical and experimental techniques. Kurt [27–29] has examined the spectroscopic features of pentafluorophenylboronic acid, 4-chloro and 4-bromophenylboronic acid molecules through density functional theory (DFT) and ab initio Hartree–Fock calculations. In addition, Kurt et al. [30] have studied the molecular structure and vibrational spectra of 3- and 4-pyridineboronic acid and carried out a NBO analysis of 3,5-dichlorophenylboronic acid

* Corresponding author.
E-mail address: eminetanis@yandex.com (E. Tanış).

https://doi.org/10.1016/j.molstruc.2017.10.057
0022-2860/

using DFT [31]. They have also investigated the geometrical and vibrational properties of 2,4-dimethoxy phenylboronic acid [32] and of 2,6- dimethoxy phenylboronic acid [33]. 2,3-difluorophenylboronic acid [34] and acenaphthene-5-boronic acid molecules [35] were performed using the theoretical and experimental studies. In addition, Rani et al. [36] have investigated the vibrational and electronic transitions and conformations of methylboronic acid. Lastly, Karabacak et al. [37] has analyzed the monomeric and dimeric structure of 3,5-difluorophenylboronic acid, and Piergies et al. [38] have carried out a spectroscopic study on positional effects of phenylboronic acids.

As far as we are aware, there is no any reports about a spectroscopic analysis of the 4-Formyl Phenyl Boronic Acid Pinacol Ester (4-FPBAPE) molecule through theoretical and experimental techniques (Fourier transform infrared spectroscopy (FT- IR), dispersive Raman, ^{13}C and ^{1}H nuclear magnetic resonance (NMR) and Ultraviolet–visible (UV–Vis) spectra). Geometrical parameters of the ground state, IR, Raman, NMR and UV spectra, HOMO-LUMO energies and MEP calculations for the title molecule are presented for the first time. Bond distances, frequencies, chemical shifts, Infrared and Raman intensities and excitation energies were calculated by using DFT/B3LYP method. This method is widely used in calculations for the similar compounds and yield reliable results [39]. Theoretical calculations for the nonlinear optic properties of 4FPBAPE, e.g., dipole moment, anisotropy of polarizability and first hyperpolarizability as well as the thermodynamic functions for the title molecule such as entropy, heat capacity and enthalpy were performed. Moreover, radial distribution functions (RDFs) and probability density depending on coordination number were recorded. The experimental results (IR, Raman, NMR and UV spectra) were found to be agreement with theoretical ones. The computed results were compatible with the theoretical results.

2. Experimental

The molecule of 4FPBAPE was purchased from Across Organics Company in solid state with a purity of above 97%. Its FT-IR and dispersive Raman spectra were recorded between 4000 and 400 cm^{-1} and 3500 -10 cm^{-1}. FT-IR spectrum was recorded at room temperature with a scanning speed of 10 $cm^{-1}min^{-1}$ and a spectral resolution of 4.0 cm^{-1} using the KBR disk method on a Perkin Elmer BX spectrometer. Dispersive Raman spectra were recorded on a Bruker RFS 100/S FT-Raman instrument using the YAG laser with a 1064-nm excitation. Its UV–Vis absorption spectrum was dissolved in ethanol and recorded in the 200–400 nm range via Shimadzu UV-2101 PC, UV–Vis recording spectrophotometer. NMR (^{1}H and ^{13}C) spectrum of 2M1HB5C was performed through Varian Infinity Plus spectrometer at 300 K. Dimethyl sulfoxide (DMSO) was chosen to dissolve the compound. Chemical shifts were stated in ppm relative to tetramethylsilane (TMS).

3. Calculations

The structural, electronic and spectroscopic properties of 4FPBAPE have been investigated using the gradient corrected DFT [40] and B3LYP [41,42], which is accepted as the most effective method. B3LYP is one of the best functions to define harmonic vibrational wavenumbers for small and medium-size molecules in

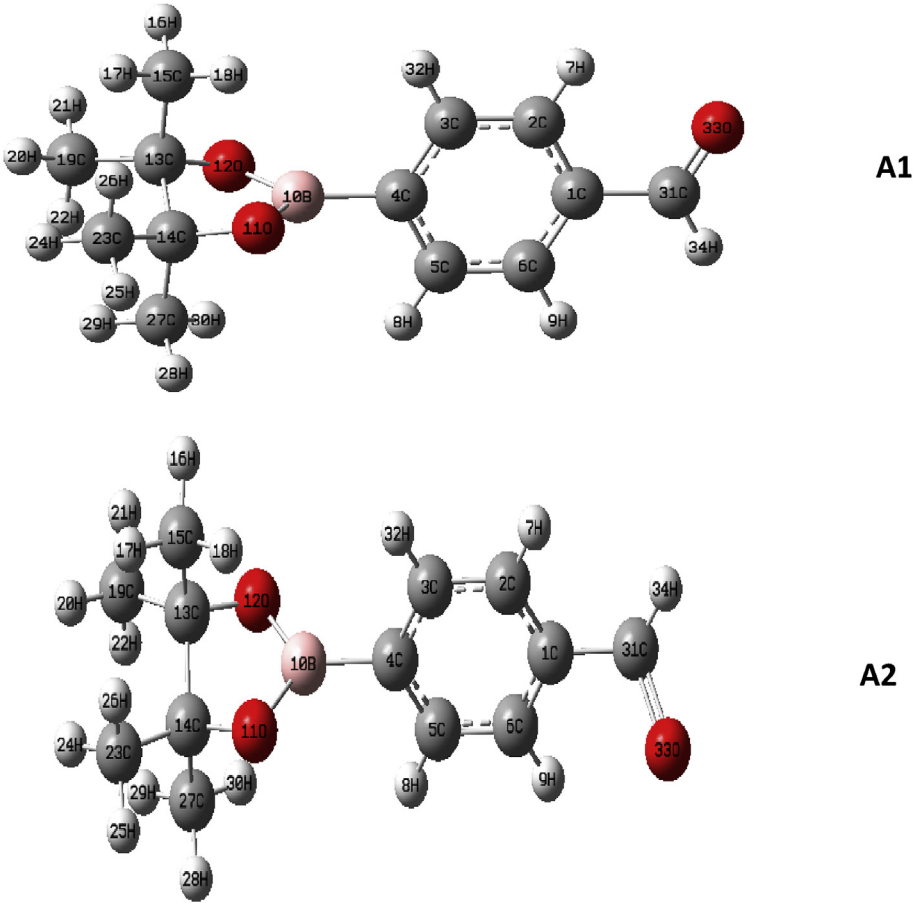

Fig. 1. Theoretical geometric conformers of the 4-Formyl phenyl boronic acid pinacol ester.

Table 1
Calculated energies and energy difference for two conformers of 4-Formyl Phenyl Boronic Acid Pinacol Ester.

Conformers	Energy		Energy differences[a]	
	Hartree	kcal/mol	Hartree	kcal/mol
A1	−756.46013369	474686.2984918119	0.01813571	11.380339
A2	−756.47282694	474694.2636331194	0000	0000

(1 a.u = 1 Hartree = 627.51 kcal/mol).
[a] Energies of the other conformer relative to the most stable A2 conformer.

the quantum chemistry. 6-311 + G (d, p) basis set has been used in the calculations. In order to test the validity and reliability of our calculations, CAM-B3LYP functional were also tested for accuracy and efficiency of the calculations. The calculations have been performed using the GAUSSIAN09 program package [43]. The optimized structural parameters were used in calculating the electronic properties, in vibrational frequency and isotropic chemical shift. As for conformational properties, the molecular energy profile was obtained with a rotation from 0° to 360° in every 10° at the selected torsional freedom degrees of T (C–C–C–O) and T(C–C–B–O). Fig. 1 shows two possible conformations (A1 and A2) of 4FPBAPE. We optimized those different conformations for the C_1 point group symmetry of 4FPBAPE molecule according to the position of oxygen atom and the scan results. According to the calculations, A2 conformation was more stable than A1 conformation, even though

Table 2
The bond length and angle values of optimized 4-Formyl Phenyl Boronic Acid Pinacol Ester.

Bond Length	4-Formyl Phenyl Boronic Acid Pinacol Ester	4-formylphenylboronic acid
C1–C2	1.40	1.40
C1–C6	1.40	1.40
C1–C31	1.54	1.48
C2–C3	1.40	1.39
C2–H7	1.07	1.08
C3–C4	1.40	1.40
C3–H34	1.07	1.08
C4–C5	1.40	1.40
C4–B10	1.65	1.57
C5–C6	1.40	1.39
C5–H8	1.07	1.08
C6–H9	1.07	1.08
B10–O11	1.54	1.39
B10–O12	1.54	1.35
O11–C14	1.43	
O12–C13	1.43	
C13–C14	1.53	
C13–C15	1.54	
C13–C19	1.54	
C14–C23	1.54	
C14–C27	1.54	
C15–H16	1.07	
C15–H17	1.07	
C15–H18	1.40	
C19–H20	1.07	
C19–H21	1.07	
C19–H22	1.07	
C23–H24	1.07	
C23–H25	1.07	
C23–H26	1.07	
C27–H28	1.07	
C27–H29	1.07	
C27–H30	1.07	
C31–O32	1.50	1.21
C31–H33	1.03	1.11
Bond Angle	**4-Formyl Phenyl Boronic Acid Pinacol Ester**	**4-formylphenylboronic acid**
C2–C1–C6	120.00	–
C2–C1–C31	120.00	119.6
C6–C1–C31	120.00	120.7
C1–C2–C3	120.00	–
C1–C2–H7	120.00	119.5
C3–C2–H7	120.00	120.1
C2–C3–C4	120.00	120.1
C2–C3–H32	120.00	120.1
C4–C3–H32	120.00	–
C3–C4–C5	120.00	–
C3–C4–B10	120.00	–
C5–C4–B10	120.00	–
C4–C5–C6	120.00	–
C4–C5–H8	120.00	120.4
C6–C5–H8	120.00	–
C1–C6–C5	120.00	–
C1–C6–H9	120.00	–
C5–C6–H9	120.00	121.4

(*continued on next page*)

Table 2 (*continued*)

Bond Length	4-Formyl Phenyl Boronic Acid Pinacol Ester	4-formylphenylboronic acid
C4–B10–O11	124.17	122.4
C4–B10–O12	124.17	119.3
O11–B10–O12	111.66	118.1
B10–O11–C14	97.48	–
B10–O12–C13	97.48	–
O12–C13–C14	103.83	–
O12–C13–C15	110.33	–
O12–C13–C19	111.93	–
C14–C13–C15	109.76	–
C14–C13–C19	112.46	–
C15–C13–C19	108.47	–
O11–C14–C13	103.83	–
O11–C14–C23	111.93	–
O11–C14–C27	110.33	–
C13–C14–C23	112.46	–
C13–C14–C27	109.76	–
C23–C14–C27	108.47	–
C13–C15–H17	109.47	–
C13–C15–H18	109.47	–
H16–C15–H17	109.47	119.6
H16–C15–H18	109.47	120.7
H17–C15–H18	109.47	–
C13–C19–H20	109.47	119.5
C13–C19–H21	109.47	120.1
C13–C19–H22	109.47	120.1
H20–C19–H21	109.47	120.1
H20–C19–H22	109.47	–
H21–C19–H22	109.47	–
C14–C23–H24	109.47	–
C14–C23–H25	109.47	–
C14–C23–H26	109.47	–
H24–C23–H25	109.47	–
H24–C23–H26	109.47	–
H25–C23–H26	109.47	–
C14–C27–H28	109.47	–
C1–C31–O33	112.23	124.8
C1–C31–H34	124.49	114.5
O33–C31–H34	107.60	–

their energies did not differ substantially. The energies and relevant differences of the two conformations [and the relative energy of the other conformation: $\Delta E = E(A1) - E(A2)$, A2 being the lowest energy as the reference point] are presented in Table 1. The results indicate that the energy of A2 conformation is 11.38 kcal/mol lower than that of A1 conformation. After ascertaining A2 as the most appropriate conformation for the studied molecule, its vibrational frequencies, Infrared, Raman intensities and UV–Vis spectra for the planar structure (C1) were calculated using the DFT/B3LYP/6-311 + G (d, p) method. In order to make the calculated vibrational frequencies more compliant with the experimental results, they were multiplied by 0.9684 as a global scaling factor for B3LYP/6-311 + G (d, p). Vibrational modes were assigned through VEDA4 program [44].

The theoretical Raman intensities of dispersion [45,46] were converted to the relative Raman intensities (I^{Ra}). ^{1}H and ^{13}C NMR isotropic chemical shifts were calculated via GIAO [47,48] with the basis set of B3LYP/6-311 + G (d, p) in DMSO, water, ethanol, and in gaseous phase. Natural bond orbital (NBO) calculations were performed to understand the intra- and intermolecular bonding of 4FPBAPE as well as the interaction between those bonds. GaussSum 2.2 program [49] was used to analyze the spectra of total density of state (TDOS or DOS), partial density of state (PDOS), overlap population density of state (OPDOS or COOP) and the group contributions of molecular orbitals. The molecular electrostatic potential (MEP) and the surface map showing the molecular electron density were evaluated and presented as 2D and 3D. Heat capacity (from 100 K to 700 K), entropy and enthalpy values for the title molecule were investigated. The dipole moment and nonlinear optic (NLO) properties of 4FPBAPE were computed and interpreted.

4. Results

4.1. Geometric optimization

The molecule in title does not have a crystal structure. The calculated geometrical parameters of 4-formylphenylboronic acid (4-CHO-PhB(OH)2) molecule [39], which is structurally similar to the optimized molecule, were therefore compared as in Table 2. The present conformations for the title molecule are seen in Fig. 1. The A2 form of 4FPBAPE molecule is presented with its atomic numbering scheme in Fig. 1. The title compound has a molecular structure containing a Boronic acid pinacol ester and formyl group attached to a benzene ring. The 4-CHO-PhB(OH)2 molecule contains a Boronic acid and formyl group attached to a benzene ring. The theoretical results of the molecule in Ref. [39] are presented in Table 2 so as to compare them with the optimized parameters (bond lengths and angles) of 4FPBAPE. Theoretical optimized geometric structure of the 4-Formyl phenyl boronic acid pinacol ester is given in Fig. 2. The results are principally in agreement with each other, albeit some differences. Those differences may result from the effects of the pinacol ester functional group attached to the benzene ring in the compared molecules. Moreover, we used the basis set of DFT/B3LYP/6-311 + G (d,p) while the calculations in

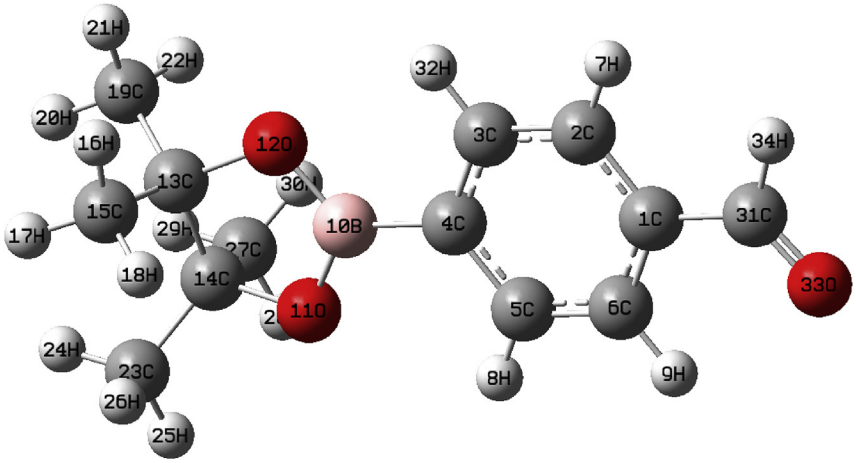

Fig. 2. Theoretical optimized geometric structure of the 4-Formyl phenyl boronic acid pinacol ester.

Ref. [39] were performed via DFT/B3LYP/6-311++G (d,p). The negligible differences, for instance, between the C–C bond lengths in the benzene ring appear to be a result of using different basis sets. While the optimized C1–C31 bond length was calculated as 1.54 Å in the present study, it was found as 1.48 Å in Ref. [39]. The bond lengths of C4–B10, B10–O11, and B10–O12 are different

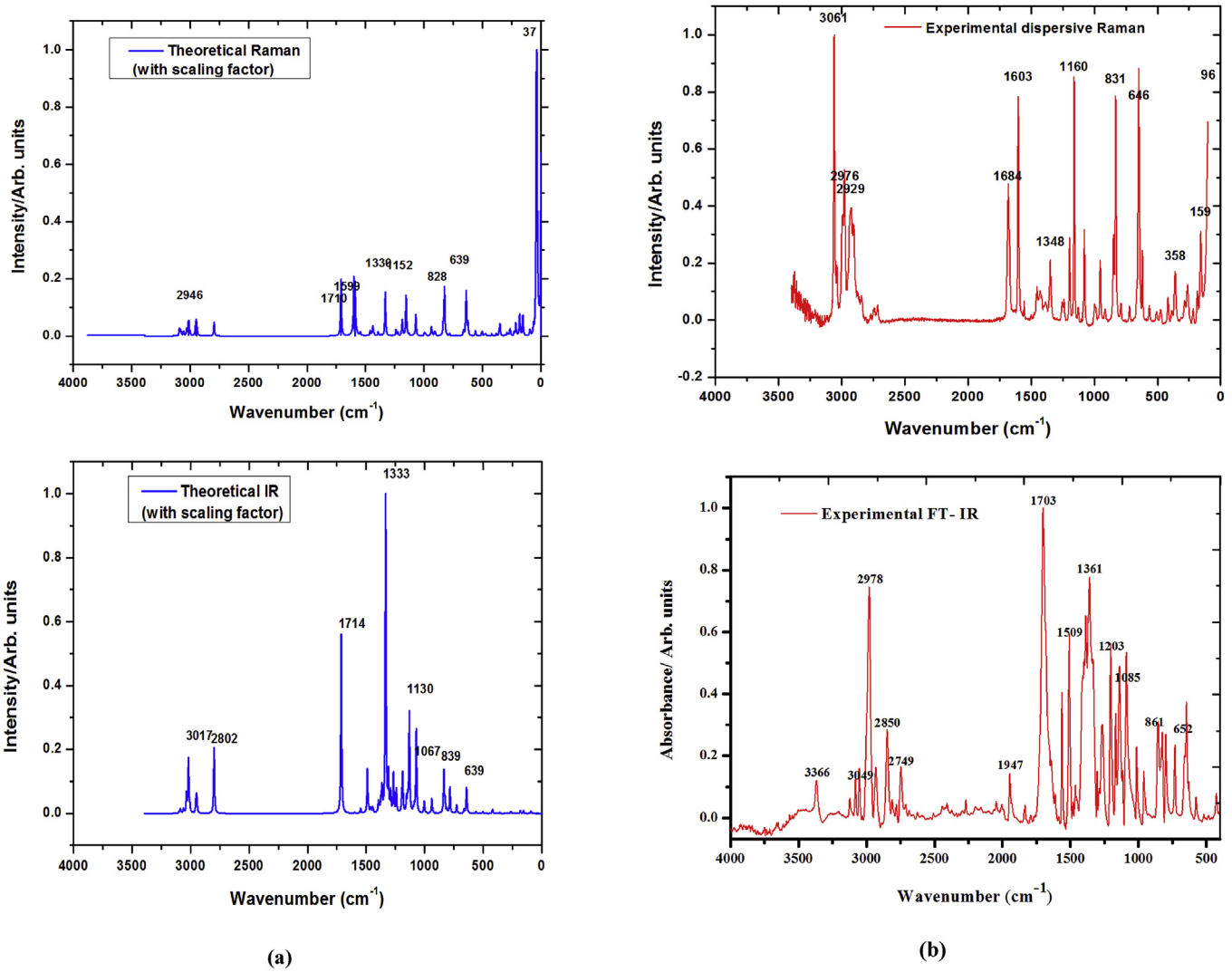

Fig. 3. a) The calculated Fourier transform infrared spectroscopy and dispersive Raman spectra of the 4-Formyl phenyl boronic acid pinacol ester b) The experimental Fourier transform infrared spectroscopy and dispersive Raman spectra of the 4-Formyl phenyl boronic acid pinacol ester.

Table 3
Comparison of the calculated and experimental vibrational spectra and proposal assignments of 4-Formyl Phenyl Boronic Acid Pinacol Ester molecule.

No	Experimental wavenumber		Theoretical wavenumber				Total Energy Distribution (10%)
	Fourier transform infrared	Dispersive Raman (780nm)	Scaled	IntensityIR	ActivityRa	IntensityRa	Assignments[a]
1			35	0.57	3.81	2.80	τCCBO (87)
2			40	0.51	4.14	2.47	τCCBO (57), τCCCB (23)
3			64	0.33	0.33	1.58	τCCCC (38), τCCCO (27)
4			91	3.50	0.13	14.85	δCCB (36), δCBO (47)
5		97	95	1.39	0.23	6.61	τCCCO (61)
6		158	156	5.15	1.87	16.27	τCCCC (10), τCCCB (28), τCOBO (10)
7			182	5.71	2.38	19.52	δCCC (46)
8			206	06	0.15	3.22	ΓCH [τCCCH (19)], τCCOH (18)
9			216	0.72	1.66	3.23	τCCCH (14), τCCOH (13), τCCCC (19)
10			230	0.92	0.49	3.25	ΓCH [τCCCH (43)], τCCOH (21)
11			260	1.41	0.22	10.06	ΓCH [τCCCH (32)]
12			265	2.77	1.08	9.76	δCCC (32), δCCO (11), τCCCH (14), τCCBO (11)
13			279	0.28	0.29	2.10	ΓCH [τCCCH (48)], τCCOH (25)
14			289	0.44	0.14	2.45	ΓCH [τCHHH (40)],
15			291	0.14	0.46	2.22	ΓCH [τCHHH (40)]
16			311	0.98	0.18	3.59	δCCC (10), τCHHH (27)
17			351	0.23	2.82	2.36	ΓCHHH (35)
18		363	359	1.84	0.90	5.98	ρCH (γCHH (25))
19			383	0.39	0.62	1.85	ρCH (γCHH (35)), τCCCC (20)
20			403	0.02	0.08	1.63	γHCCH (12)
21			420	7.76	0.67	25.02	γHCCH (12), γCH(12), τCCBO(14)
22			473	0.89	0.69	3.45	τCCCC (15), τCCCH (17)
23			481	0.16	0.53	1.46	τCCCC (24)
24			503	2.93	1.42	10.62	γCHH (35), τCCBO (11)
25			508	0.59	0.76	5.31	ρCH (γCHH (35)), τCCBO (28)
26			560	3.34	2.28	11.33	ρCH (γCHH (42)), τCCBO(28)
27			625	1.66	6.52	16.46	τCCCC (66), δCCO (18)
28			640	13.72	23.60	175.59	τCCCC (16), γCCHH (43)
29	652	642	642	39.08	0.31	150.58	τCCCC (16), τCOBO(15),γ CH(22)
30			662	7.01	2.72	30.45	τCCCC(34), τCCBO (13), δCCC (15), δCCO (14)
31			726	16.20	0.47	55.22	τCCBH (14), γCCC (33), γCH(13)
32			783	51.87	1.39	151.83	γCH [ρCCH (45)], γCOBO (35), γCCC (10)
33			810	7.38	0.53	39.68	δCCO (10), ΓCCHH(38)
34			820	13.93	16.41	56.70	τCOBO (13), τCCCH(13)
35			825	9.05	20.81	120.33	γCH (10),CCCC (12), δCOB (11)]
34		833	835	83.14	9.64	289.09	υCO (37), γCCC (10)
37	861		849	1.82	0.08	28.81	γCH (63)
38			904	0.50	1.87	4.58	ρCH (γCHH (38))
39			909	0.01	3.49	3.96	CHH (53)
40			930	2.46	2.51	32.13	ρCH (γCHH (25))
41			938	27.85	8.22	94.12	ρCH (γCHH (41)), τCCCC(14)
42			959	0.03	0.2	4.92	γCH[τCCCH(42),τCHCH(41)]
43			981	0.0	0.33	6.1	ΓCCH (62)
44			982	0.05	0.85	6.44	ρCH (γCHH (25))
45			991	0.16	2.37	14.37	ρCH (γCHH (28))
46			998	1.33	2.70	60.61	γ CH(18)
47			1002	23.15	0.25	84.65	τCCHH (63)
48			1070	165.21	25.60	528.72	υCC (11), υBO (33), δCCC (28), δCCH (19)
49	1085		107	12.66	1.11	69.09	υBO (10), δCH [ΓCCH (21)]
50			1096	6.84	0.96	49.06	υBO (10), δCH [ΓCCH (52)]
51			1129	197.73	2.48	645.21	υCO (12), γCCH (38)
52			1143	27.17	2.05	152.73	ρCH (γCHH (15))
53		1159	1154	28.81	55.46	105.53	υCC (19), δCH [ΓCCH (80)]
54			1187	74.68	22.54	207.44	υCC (42), δCH [ΓCCH (35)]
55	1203		1194	24.49	2.19	121.52	γCHH (14)
56			1224	0.05	5.75	21.35	ρCH (γCHH (35))
57			1241	45.83	9.64	157.20	υCC (30), γCHH (44)
58			1265	76.86	0.96	263.85	υCC(36),δCCH (18),δOBO(32)
59			190	3.48	0.78	160.12	ΓCCH(32),ΓCCHH(40)
60			1307	73.95	0.18	318.76	υCC (40), υBO (53), υCH(14)
61			1332	627.98	79.40	1987.77	υCB (59), υBO (31), ΓCHCH(12)
62			1360	1.34	0.26	153.24	ρCH[δCHH (44)]
63	1361		1364	26.91	0.38	205.56	ρCH[δCHH(45)]
64			1365	2123	1.66	189.52	δCCH (24), ρCH[δHH (37)]
65			1373	20.12	0.71	117.21	δCCH (14), ρCH[δCHH (46)]
66			1384	6.11	0.46	58.88	ρCH[δCHH (23)]
67			1393	21.02	7.74	81.16	υCC (24), δCCH (65)
68			1426	0.02	4.18	11.41	ρCH[δCHH (52)]
69			147	2.58	0.87	31.21	ρCH[δCH (48)]
70			1438	0.43	727	33.97	ρCH[δCHH (45)]
71			1443	9.58	6.62	44.01	ρCH[δCHH (50)]
72			1455	5.37	3.10	38.58	ρCH[δCHH (49)]
73			1460	3.39	4.46	43.49	ρCH[δCHH (51)]

Table 3 (*continued*)

No	Experimental wavenumber		Theoretical wavenumber				Total Energy Distribution (10%)
	Fourier transform infrared	Dispersive Raman (780nm)	Scaled	IntensityIR	ActivityRa	IntensityRa	Assignments[a]
74			1461	4.23	5.26	41.63	ρCH[δCHH (43)]
75			1476	680	0.70	60.16	ρCH[δCHH (40)]
76			1488	86.44	0.91	281.63	ΓCCHH(40), υCB (14), υCC(36)
77	1509		1545	9.42	7.97	30.55	υCC(62), δCCH(15), δCOH(14)
78		1597	1596	2.00	486.62	8.69	υCC(66), δCCH(15), υCB(10)
79	1703	1675	1711	353.60	206.50	1113.26	υCO(85)
80	2749		2796	129.57	167.84	431.55	υCH(100)
81	285		2941	2.76	3.77	115.94	υCH(100)
82			2943	20.83	3.55	137.97	υCH(93)
83	2850		2945	9.74	6.80	136.03	υCH(95)
84		2933	2950	26.64	579.23	112.81	υCH(100)
85	2978	2984	3003	2.50	29.08	87.99	υCH(97)
86			004	8.1	12.50	92.82	υCH(100)
87	3049		3010	1.25	5.10	232.18	υCH(95)
88			3012	10.67	47.46	336.86	υCH(96)
89			3014	51.61	58.00	380.18	υCH(100)
90			3015	47.58	132.75	292.63	υCH(97)
91			3030	16.75	65.85	150.81	υCH(97)
92			3031	21.51	42.95	135.50	υCH(85)
93			3057	8.24	72.63	32.42	υCH(100)
94			376	2.02	46.78	17.71	υCH(100)
95			3084	7.87	85.60	27.45	υCH(100)
96			3094	2.83	119.30	13.34	υCH(100)

[a] υ stretching. δ: in plane bending. γ: out of plane bending. Γ: torsion ρ: scissoring.

likewise than the values in Ref. [39], with 0.19 Å being the greatest deviance observed in the B10–O12 bond length. These results may be from the Boronic acid pinacol ester group attached to a benzene ring in this study. For the 4FPBAPE molecule, C–H bonds are almost the same with those in Ref. (39). The bond angles of the optimized benzene ring are in compatible with the experimental values. For example, C2–C1–C31 angle was calculated as 120° in this study and as 119.6° in Ref. [39]. This agreement is observed on the C–C–C bonds in the benzene ring as well.

4.2. Vibrational spectral analysis

The molecule has 96 modes of fundamental vibration with C_1 symmetry. The measured and calculated IR and dispersive Raman spectra of the molecule are presented in Fig. 3. All those calculations were conducted in gaseous phase. However, the experimental results were taken for the solid sample, which accounts for the disagreement between the experimental and calculated wavenumbers to a certain extent and the situations like not observing the calculated results in the experimental ones. Vibrational frequencies were calculated using the basis set of DFT/B3LYP/6-311 + G (d, p) [43] and 0.9684 was taken as the scaling factor for 6-311 + G (d, p). The calculated and experimental vibrational frequencies are listed in Table 3. Fig. 4 shows the correlation graphics for experimental and theoretical wavenumbers.

4.3. Phenyl ring vibrations

In the literature, C–H stretching vibration in aromatic compounds is observed in the range of 3000–3100 cm^{-1} [50]. Phenyl ring has four aromatic C–H bonds in this molecule. The stretching vibration of these bonds was calculated in the range of 3057–3094 cm^{-1} using B3LYP/6-311 + G(d,p), with 3057, 3076 cm^{-1} being asymmetric stretching vibration and 3084, 3094 cm^{-1} symmetric stretching vibration. According to the PED column of the table, molecular C–H stretching vibrations are in quite pure bands. In aromatic compounds, plane bending vibrational frequencies are observed between 1000 and 1300 cm^{-1} while out-of-plane bending vibrational frequencies are seen between 750 and 1000 cm^{-1} [50,51]. Plane bending vibrational frequencies for this molecule were calculated in the range of 1002, 1087, 1096, 1154, 1187 cm^{-1}; FT-IR and dispersive Raman were observed at 1085 cm-1 and 1159 cm-1, respectively. The out-of-plane bending vibrations were calculated in the range of 959, 981, 998 cm^{-1}. Whereas the pinacol ester group attached to the phenylboronic acid molecule increases C–H stretching vibrations, the formyl group attached to the molecule decreases the mentioned vibrations.

CC ring stretching vibrations are significant and characteristic for the aromatic ring. Varsanyi [52] has observed the CC stretching band in different densities in the range of 1625–1590, 1575-1590, 1470-1540, 1430-1465 and 1280-1380 cm^{-1}. The CC stretching band for 4FPBAPE was calculated as 1596,1545, 1393,1307, 1265,1241, 1194–1154, 1096–1070, 825 cm^{-1} using the B3LYP method.

4.4. Methyl group vibrations

Methyl (CH_3) asymmetric stretching vibrations for 4FPBAPE molecule were calculated between 3003 and 3031 cm^{-1}; FT-IR and dispersive Raman were observed at 2978, 3049 cm^{-1} and 2984 cm

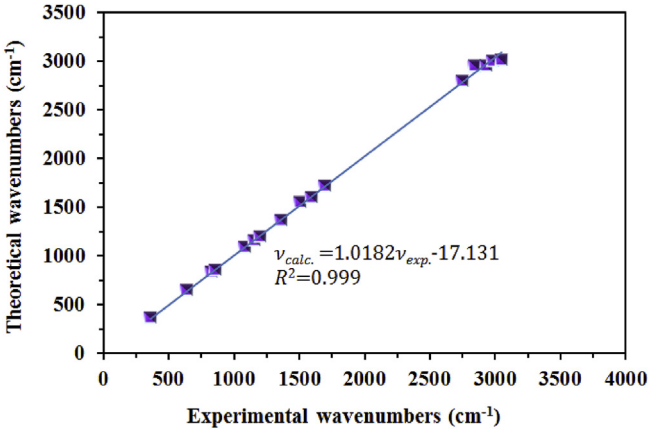

Fig. 4. Correlation graphic of calculated and experimental frequencies for 4-Formyl phenyl boronic acid pinacol ester.

Table 4
Second order perturbation theory analysis of Fock matrix in NBO basis for 4-Formyl Phenyl Boronic Acid Pinacol Ester. E(2): Energy of hyper conjugate interaction (stabilization energy), E(j)-E(i): Energy difference between donor and acceptor i and j NBO orbitals, F(i,j): The Fock matrix element between i and j NBO orbitals.

Donor (i)	Type	ED/e	Acceptor(j)	Type	ED/e	E(2) (KJ mol^{-1})	E(*j*)–E(i) (a.u)	F(i,j) (a.u)
C1–C2	π	1.64	C3–C4	π*	0.34	18.32	0.2	0.065
C1–C2	π	1.64	C5–C6	π*	0.29	1875	0.29	0.0
C1–C2	π	1.64	C31–033	π*	0.09	12.48	0.25	0.053
C1–C6	σ	1.98	C1–C2	σ*	0.02	3.62	1.26	0.06
C1–C6	σ	1.98	C2–H7	σ*	0.01	2.29	1.15	0.046
C1–C31	σ	1.98	C5–C6	σ*	0.02	2.36	1.21	0.048
C2–C3	σ	1.97	C1–C2	σ*	002	3.14	126	0.056
C2–C3	σ	1.97	C1–C1	σ*	0.04	34	1.06	0.056
C2–C3	σ	1.97	C4–B10	σ*	0.03	3.35	1.07	0.053
C2–H7	σ	1.98	C1–C6	σ*	0.02	4.33	1.09	0.061
C3–C4	σ	1.97	C4–C5	σ*	0.02	3.17	1.26	0.057
C3–C4	π	1.64	C1–C2	π*	0.37	21.35	0.27	0.069
C3–C4	π	1.64	C5–C6	π*	0.29	18.09	0.28	0.065
C3–H3	σ	1.98	C1–C	σ*	0.02	3.39	1.09	0.054
C4–C5	σ	1.97	C3–C4	σ*	0.02	3.17	1.26	0.056
C4–B10	σ	1.97	C2–C3	σ*	0.01	3.92	1.09	0.059
C4–B10	σ	1.97	C5–C6	σ*	0.01	3.89	1.09	0.058
C4–C5	σ	1.97	C4–B10	σ*	0.03	3.39	1.06	0.054
C5–C6	π	164	C1–C2	σ*	0.02	20.63	0.27	0.067
C5–C6	π	1.64	C3–C4	σ*	0.02	21.82	0.28	0.07
C5–H8	σ	1.98	C3–C4	σ*	0.02	4.07	1.09	0.059
C6–H9	σ	1.98	C1–C2	σ*	0.01	4.37	1.08	0.061
C31–O33	π	1.97	C1–C2	σ*	0.02	5.25	0.41	0.045
B10	LP*(1)	0.45	C4–B10	π*	0.03	8.57	0.33	0.097
C3–C4	π*	0.34	B10	LP*(2)	0.34	23.55	0.08	0.068
O11–C14	σ	1.98	B10	LP*(1)	0.45	24.17	0.89	0.148
O11–C14	σ	1.98	B10	LP*(2)	0.34	11.34	0.96	0.102
O12–C13	σ	1.98	B10	LP*(1)	0.45	24.02	0.89	0.147
O12–C13	σ	1.98	B10	LP*(2)	0.34	11.48	0.96	0.102
O11	LP(1)	1.96	B10	LP*(2)	0.45	18.74	0.7	0.111
O11	LP(3)	1.62	B10	LP*(1)	0.45	173.67	0.52	0.273
O11	LP(3)	1.62	B10	LP*(2)	0.34	115.99	0.59	0.236
O12	LP(1)	1.96	B10	LP*(2)	0.45	18.77	0.7	0.111
O12	LP(2)	1.83	B10	LP*(3)	0.28	30.45	0.28	0.084
O12	LP(3)	1.62	B10	LP*(1)	0.45	172.21	0.52	0.272
O12	LP(3)	1.62	B10	LP*(2)	0.45	116.84	0.59	0.237

$^{-1}$, respectively. CH_3 shear vibrations were calculated theoretically as 1360, 1364, 1373, 1384, 1426-1476 cm^{-1}, and FT-IR was observed at 1361 cm^{-1}. PED contribution of these bands are mostly pure and related to the other modes in certain vibrations. The aforementioned results are consistent with the results for the similar molecules in the literature [27–29].

4.5. Ring vibrations

C–C and C=C vibrations usually occur in the range of 1430–1625 cm^{-1} in rings [53–55]. Varsanyi [52] has observed this C–C stretching band as five ranges in the frequency regions of 1625–1590, 1575-1590, 1470-1540, 1430-1465 and 1280-1380 cm^{-1}. The C–C phenyl ring stretching vibrations for 4FPBAPE were calculated as 1596–1488, 1393, 1307, 1265, 1194-1154 cm^{-1} using the B3LYP method. They were measured at 1509, 1203 cm^{-1} in FT-IR spectrum and 1597, 1159 cm^{-1} in dispersive Raman spectrum. The greatest contribution of C–C stretching vibration was seen at 1596 cm^{-1} with a 66% PED contribution. These results are found to be compatible the experimental values. The band mode of C–C–C in-plane bending vibration is generally seen between 1000 and 600 cm^{-1} [52]. In the present study, this band was calculated as 835, 783, 726, 662 cm^{-1} and was observed at 833 cm^{-1} in dispersive Raman spectrum using the B3LYP method.

4.6. Carbon-Bor modes

In the present study, C–B stretching modes were calculated between 1332, 1488 cm^{-1} using the B3LYP/6-311 + G(d,p). The greatest contribution was observed at 1332 cm^{-1} with a 59% PED contribution. There was an agreement between the theoretical and experimental results.

Faniran et al. [25] has assigned this band for normal and deuterated phenylboronic acids at 1089 and 1085 cm^{-1}, respectively, and observed at 1354 cm^{-1} for diphenyl phenylboronate. It was observed as 701 cm^{-1} in FT-Raman, 708 cm^{-1} and 1354 cm^{-1} in FT-IR for 2-flourophenylboronic acid by Erdogdu et al. [26].

4.7. Carbon = Oxygen and Carbon–Oxygen vibrations

C=O double bond is made up of a $\pi - \pi$ bond between carbon and oxygen. Bond electrons do not show an equal distribution between C and O atoms due to their difference in electronegativity [56]. Carboniferous compounds generally have an intense and narrow peak in the range of 1800–1600 cm^{-1} [51,53]. These compounds have two strong characteristic bands of absorption, namely C=O and C–O. C=O stretching vibrations occur in higher frequencies than C–O stretching vibrations. Three C–O stretching vibrations (e.g. C13–O12, C14–O11, C31 = O33) were expectable in this study. C31 = O33 band was observed as a single band at 1703 cm^{-1} in FT-IR spectrum, at 1675 cm^{-1} in dispersive Raman, and it was assigned at 1711 cm^{-1} with a 85-% PED contribution through the basis set of B3LYP/6-311 + G(d,p). C13–O12 and C14–O11 bands were theoretically calculated at 835, 1129 cm^{-1} and observed at 833 cm^{-1}. The theoretical value was in agreement with the experimental data.

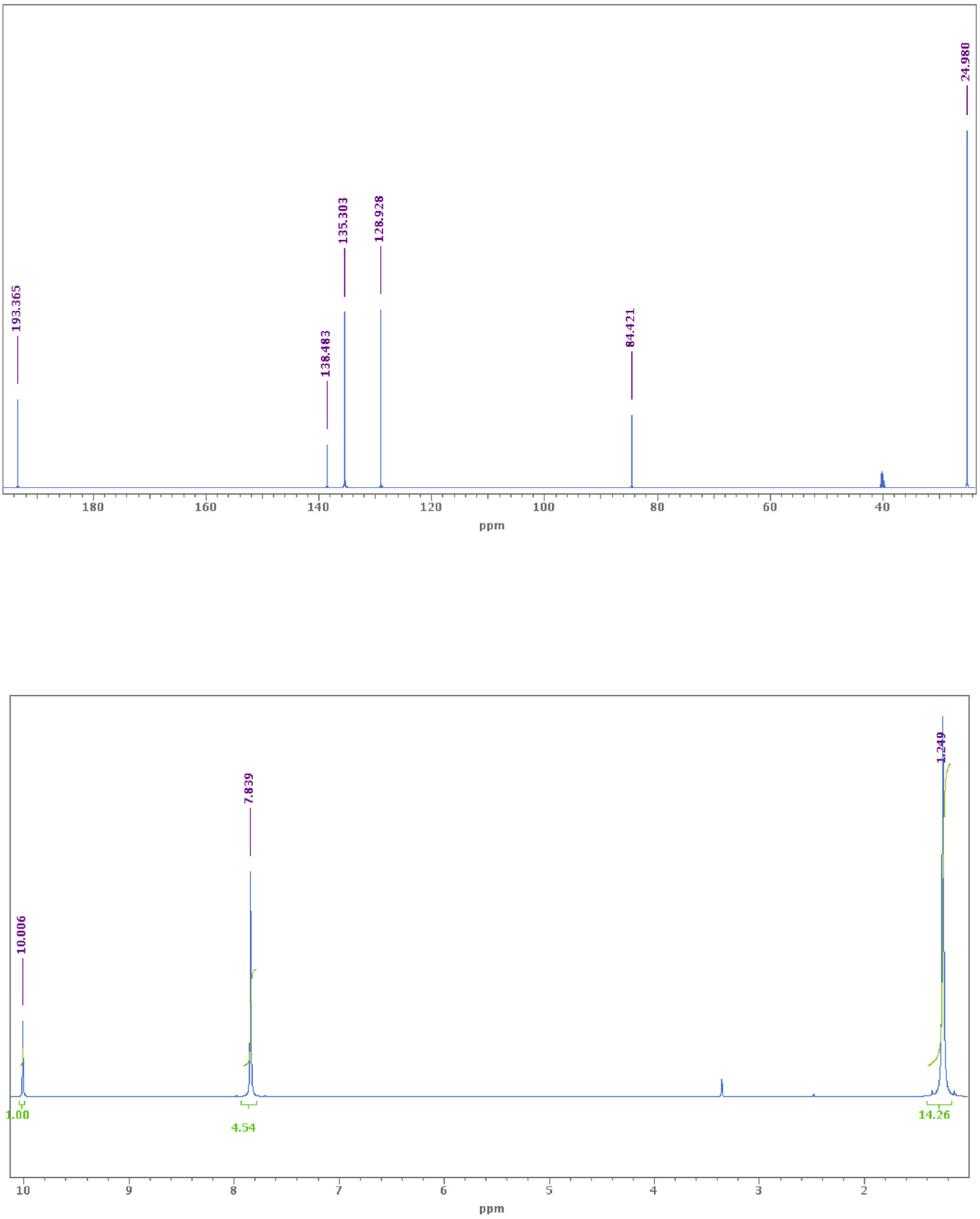

Fig. 5. [1]Hydrogen and [13]Carbon nuclear magnetic resonance spectra of the 4-Formyl phenyl boronic acid pinacol ester in Dimethyl sulfoxide solution.

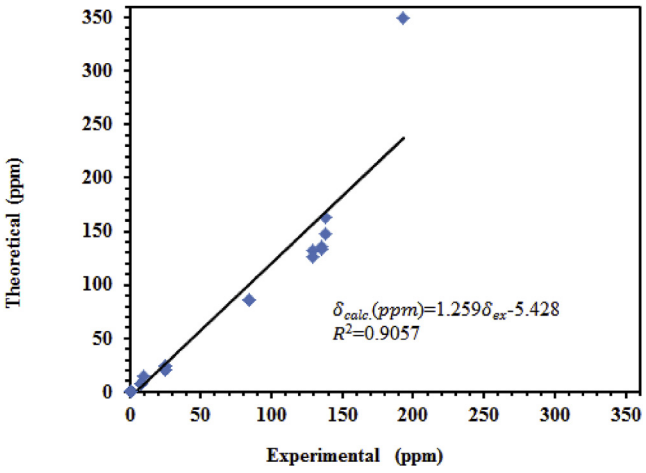

Fig. 6. Correlation graphic of calculated and experimental (total) chemical shifts of the 4 Formyl phenyl boronic acid pinacol ester.

5. Natural bond orbital analysis

A NBO analysis at DFT/B3LYP/6-311 + G(d,p) level was conducted to find out the interaction between the filled (i) and vacant orbitals (j) with the purpose of delocalization and rehybridization of intramolecular electron density for the title molecule. The result data were tabulated as presented in Table 4. The delocalization of electrons between the filled Lewis-type NBO orbitals and vacant non-Lewis NBO orbitals is associated with a stabilized donor-acceptor interaction.

The strong intramolecular hyperconjugative interaction is observed as a low stabilization energy of 3.62 and 2.29 kJ/mol in transition from C1–C6 σ bond to C2–H7 σ* anti-bond orbital.

Likewise, it results with a strong delocalization energy of 18.32 and 18.75 kJ/mol in transition from C1–C2 π bond to C3–C4 π* anti-bond and C5–C6 π* anti bond.

The paramount interaction energy with regard to the molecular resonance occurs with the transition of electrons from O11 LP(3) atom to B10 LP*(1) orbital, leading a high stabilization energy of 173.67 kJ/mol.

The transition from σ (C4–B10) bond to σ* (C5–C6) anti-bond with a low 3.89 kJ/mol stabilization energy and from π C31–O33 bond to σ* (C1–C2) anti-bond with a low 5.25 kJ/mol stabilization energy indicates not being stable enough to cause a change in phenyl ring.

6. Nuclear magnetic resonance analysis

One of the most crucial techniques to analyze organic compounds structurally is chemical shift analysis. NMR spectroscopy and computer simulation techniques are used in tandem to interpret the biomolecular structures [49]. This common and useful technique was hence employed to obtain more information about the molecule of interest. Following the geometric optimization of 4FPBAPE, its ^{1}H and ^{13}C NMR shifts were calculated with the GIAO method [47,48] and B3LYP functional 6-311 + G(d,p) basis set in water, ethanol and DMSO solvents, and in gas phase. The experimental ^{1}H, ^{13}C spectra of the molecule were taken in DMSO and are presented respectively in Fig. 5a and b. The correlation between the experimental and theoretical chemical shifts via DFT/B3LYP is presented in Fig. 6.

Chemical shifts of aromatic protons in organic compounds are mostly detected in the range of 7.00–8.00 ppm, although they vary according to the electronic environment of proton. A hydrogen attached to an electron-accepting atom or group may lead to a

Table 5
Experimental and calculated chemical shifts of 4-Formyl Phenyl Boronic Acid Pinacol Ester.

Atom	Calculated			Experimental
	Dimethyl sulfoxide	Etanol	Gas	Dimethyl sulfoxide
C31	349.60	349.61	349.73	193.19
C1	163.29	163.27	162.84	138.46
C4	147.57	147.55	146.65	138.46
C5	136.06	136.04	135.46	135.29
C3	133.49	133.43	133.30	135.29
C6	132.83	132.86	131.99	128.93
C2	126.11	126.01	123.56	128.93
C14	85.80	85.77	85.11	84.41
C13	85.71	85.68	85.05	84.41
C15	24.11	24.12	24.32	25.04
C27	23.98	23.99	24.17	25.04
C19	20.46	20.46	20.57	25.04
C23	20.43	20.43	20.54	25.04
H34	14.69	14.71	15.28	10.00
H9	7.91	7.90	7.82	7.84
H8	7.64	7.63	7.41	7.84
H32	7.50	7.49	7.21	7.84
H7	7.36	7.35	7.03	7.84
H17	0.98	0.98	0.84	1.25
H29	0.96	0.96	0.81	1.25
H30	0.87	0.87	0.85	1.25
H22	0.87	0.87	0.85	1.25
H26	0.86	0.85	0.82	1.25
H18	0.84	0.84	0.82	1.25
H20	0.64	0.64	0.44	1.25
H21	0.64	0.63	0.65	1.25
H24	0.63	0.62	0.42	1.25
H25	0.61	0.61	0.63	1.25
H16	0.58	0.57	0.53	1.25
H28	0.57	0.57	0.54	1.25

Table 6
The computed and experimental absorption wavelength λ (nm), excitation energies E(eV), oscillator strengths (f) and absorbance of 4-FPBAPE molecule.

TD-DFT/B3LYP									TD-DFT/CAM-B3LYP			Exp.	
DMSO			Gas			Ethanol			Ethanol			Ethanol	
λ	E	f	λ	E	f	λ	E	f	λ	E	f	λ	E
575.81 (59→63) (62→63)	2.15	0.0035	633.03 (60→63) (61→63) (62→63)	1.95	0.0013	577.56 (59→63) (62→63)	2.14	0.0034	553.32 (59→63)	2.24	0.0016	527.18	0.0377
394.31 (59→63) (60→63) (61→63)	3.14	0.0076	368.92 (59→63) (60→63) (61→63)	3.36	0.0043	393.59 (59→63) (61→63)	3.15	0.0072	336.63 (59→63) (62→63)	3.68	0.1961	370.86	0.0536
376.18 (59→63) (60→63)	3.29	0.1788	362.49 (59→63) (60→63)	3.42	0.1391	375.48 (59→63) (60→63)	3.30	0.1755	313.95 (59→63) (61→63) (62→63)	3.94	0.0127	298.19	0.0666

decrease in chemical shift. When proton resonance move towards to high frequencies, on the other hand, a hydrogen attached to an electron-donating atom or group increases the shift and the resonance shifts to low frequencies [57,58]. H34 NMR chemical shift value of the molecule was computed as 14.69, 14.71, and 15.28, ppm for DMSO, ethanol, and gas, respectively (see Table 5). This deviance from the ranges stated in the literature may be explained by C31 atom attached to H34 atom. Similarly, chemical shifts of H17, H29, H30, H22, H26, H18, H20, H21, H24, H25, H16, H28 atoms are likely to have been measured lower than the values in the literature because of the density in their environmental electron charges. The other values regarding the H NMR chemical shifts are within the normal range and in agreement with the literature.

Aromatic carbons usually signal in overlapping areas of the spectrum with ^{13}C NMR chemical shift values ranging from 100 to 150 ppm [59,60]. The studied molecule has thirteen C atoms in total, six of which are in phenyl ring, one in the formyl group, and

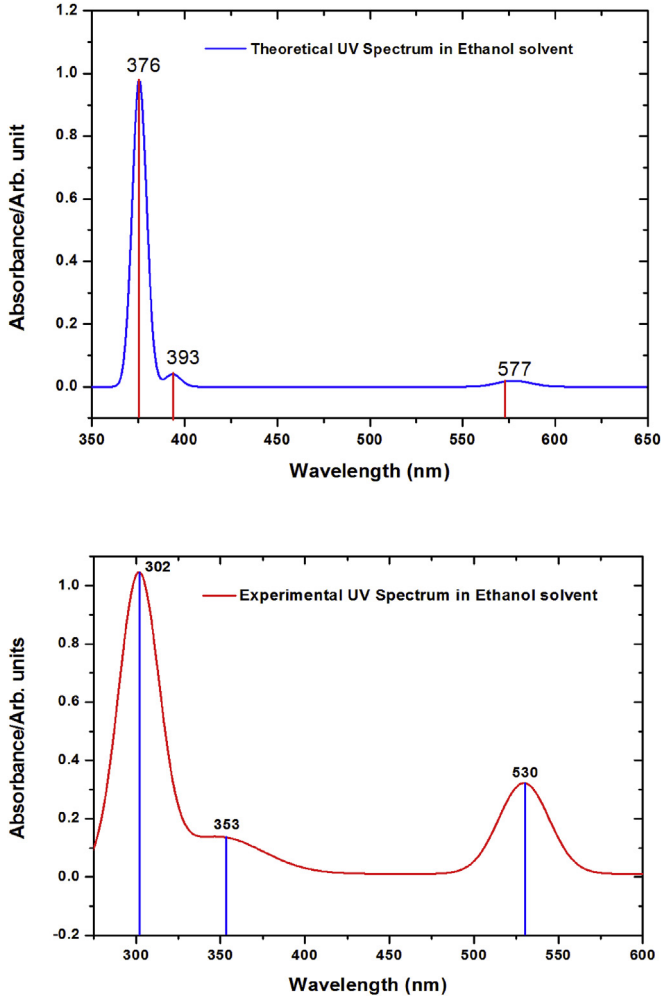

Fig. 7. The theoretical obtained from B3LYP functional and experimental Ultraviolet–visible spectrum (Dimethyl sulfoxide) of the 4-Formyl phenyl boronic acid pinacol ester.

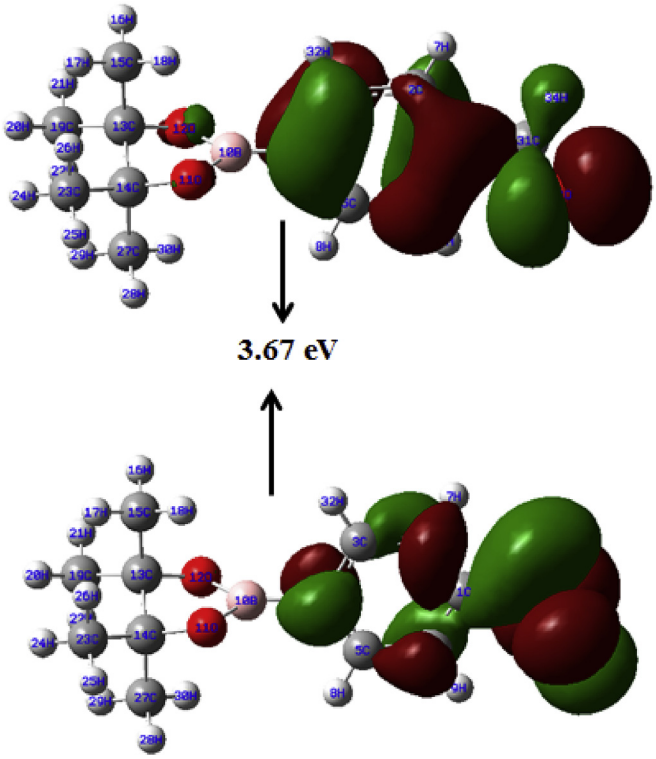

Fig. 8. The frontier molecular orbitals of the 4-Formyl phenyl boronic acid pinacol ester for gas phase.

Table 7
The calculated energy values of 4-FPBAPE using TD-DFT/B3LYP and CAM-B3LYP method with 6-311 + G(d,p) basis set.

C1symmetry	Gas	Gas(CAM-B3LYP)	DMSO	Ethanol
E_{total} (Hartree)	−756.30	−755.90	−756.31	−756.31
E_{HOMO} (eV)	−7.15	−8.86	−7.38	−7.38
E_{LUMO} (eV)	−3.47	−2.34	−3.68	−3.67
E_{HOMO-1} (eV)	−7.57	9.04	−7.59	−7.59
E_{LUMO+1} (eV)	−1.10	−0.14	−1.13	−1.13
$E_{HOMO-1-LUMO+1}$ gap (eV)	6.47	8.90	6.47	6.47
$E_{HOMO-LUMO}$ gap (eV)	3.67	6.52	3.70	3.70
Chemical hardness (h)	1.84	3.26	1.85	1.85
Electronegativity (χ)	−5.31	−5.60	−5.53	−5.54
Chemical potential (μ)	5.31	5.60	5.53	5.54
Electrophilicity index (ω)	−7.67	4.81	8.27	8.28

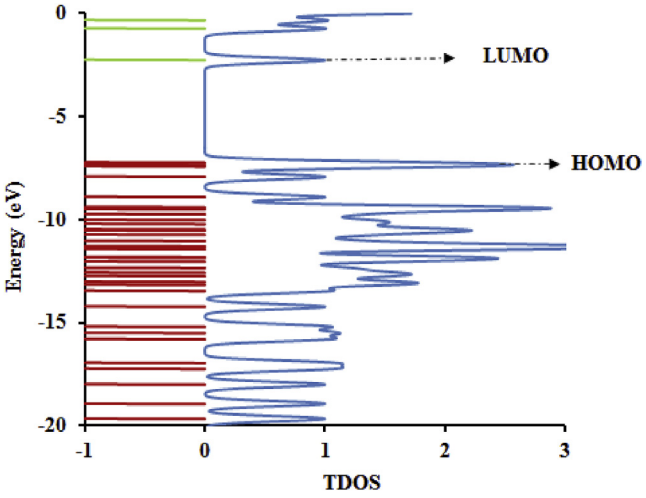

Fig. 9. The total electronic density of states diagram of the 4-Formyl phenyl boronic acid pinacol ester.

six in the pinacol ester group of Boronic acid. Except the C atoms that are bonded to the phenyl ring functional groups, all of them are in agreement with each other and the literature. C31 atoms in the formyl group were theoretically calculated at 349.60, 349.61, 349.73 ppm for DMSO, ethanol, and gas, respectively. Experimentally, it was calculated at 193.19 ppm. The C chemical shift values of the C1 atom bonded to the formyl group regarding the Boronic acid and CH_3 groups were in agreement with each other as well as the values in the literature.

7. Electronic properties

7.1. Ultraviolet–visible analysis

The electronic absorption spectra of the molecule were calculated in DMSO, ethanol and gas phase with the basis sets of TD-DFT/B3LYP/6-311 + G (d, p) and TD-DFT/CAM-B3LYP/6-311 + G (d, p). The experimental and theoretical absorption wavenumbers, excitation energies and electronic properties of the molecule are presented in Table 6. The energy values for CAM-B3LYP functional are found to be more compatible with the experimental results (see Table 6). The electronic absorption spectra for measured and predicted values in DMSO solvent are presented in Fig. 7. As it is seen there, the experimental electronic absorption spectra are compatible with theoretical results, being measured in three bands as 298.19, 370.86, 527.18 nm in DMSO.

7.2. Frontier molecular orbitals analysis

The highest occupied molecular orbital (HOMO) is related to electron-donating potential while the lowest unoccupied molecular orbital (LUMO) is relevant to electron affinity [61]. The difference between HOMO-LUMO values (energy gap) is an important parameter in determining the electrical properties of a molecule. The energy gap accounts for the molecular chemical stability and intramolecular charge transfer as well. It determines the energy required for the transition from the most stable fundamental state to an excited state in a molecule [62]. The energy gap, HOMO and LUMO are shown in Fig. 8.

HOMO orbitals were settled in the whole molecule except for the pinacol ester group and LUMO orbitals were settled in the whole molecule except for the boronic acid pinacol ester group. The calculated HOMO, LUMO and HOMO-LUMO energy values for both B3LYP and CAM-B3LYP functionals were tabulated in Table 7. The calculated HOMO-LUMO energy gap with CAM-B3LYP are found to change dramatically (approximately 2-fold) compared to B3LYP. In

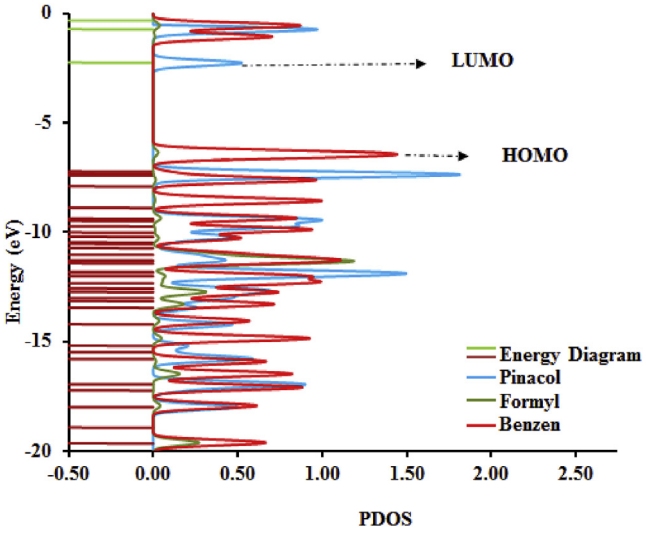

Fig. 10. The partial electronic density of states diagram of the 4-Formyl phenyl boronic acid pinacol ester.

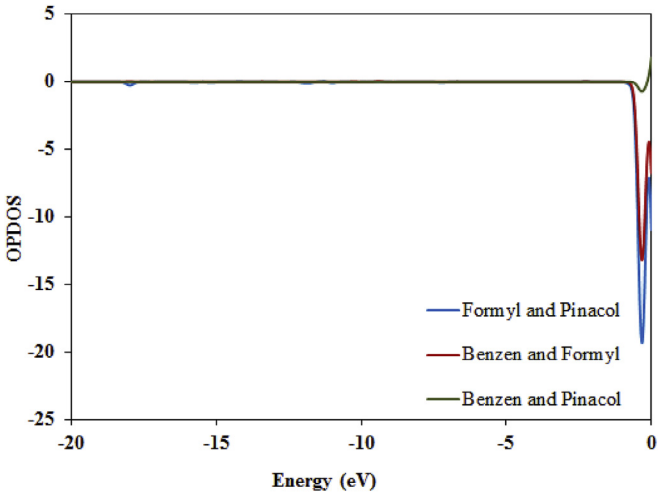

Fig. 11. The overlap population electronic density of states diagram of the 4-Formyl phenyl boronic acid pinacol ester.

addition, some electronic parameters like chemical hardness were calculated in gas phase (see Table 7).

7.3. Total, partial, and overlap population density-of-states

The orbitals close to each other in the frontier region may have semi-degenerate energy levels. Paying regard to only HOMO and LUMO in such cases may not contribute to the actual definition of frontier orbitals. Therefore, TDOS, PDOS and OPDOS density of states [63–65] were calculated and formed via GaussSum2.2 program [49]. TDOS, PDOS and OPDOS graphs are presented in Figs. 9–11. OPDOS diagrams show the interaction of two orbitals in terms of bonding (positive region), anti-bonding (negative region), and non-bonding (zero region) nature in atoms or groups [65]. The OPDOS diagram helps us not only to ascertain the bonding and non-bonding orbitals but also to compare and determine the donor-acceptor features of the ligand.

PDOS basically consists of a combination of separate orbitals contributing to the molecular orbitals. While HOMO orbitals spread over phenylboronic acid ($C_6H_5B(OH)_2$ group) and formyl (COH group), LUMO orbitals were localized on the benzene ring (C6H5 group) and formyl (COH group). However, it is difficult to know about the bonding and anti-bond features according to the percentage shares of molecular fragments or atomic orbitals in the molecule. An OPDOS diagram showing some of the orbital energy values between the particular groups were plotted, therefore, as in Fig. 11. It shows the positive (bonding) interaction between the benzene ring with the pinacol group (green line), the negative (anti-bonding) one between the formyl group and the benzene ring (red line), and the near-zero (non-bonding) one between the formyl and the pinacol group (blue line).

7.4. Molecular electrostatic potential

The molecular MEP surface diagrams are useful in understanding the physicochemical structure of a molecule since it shows the

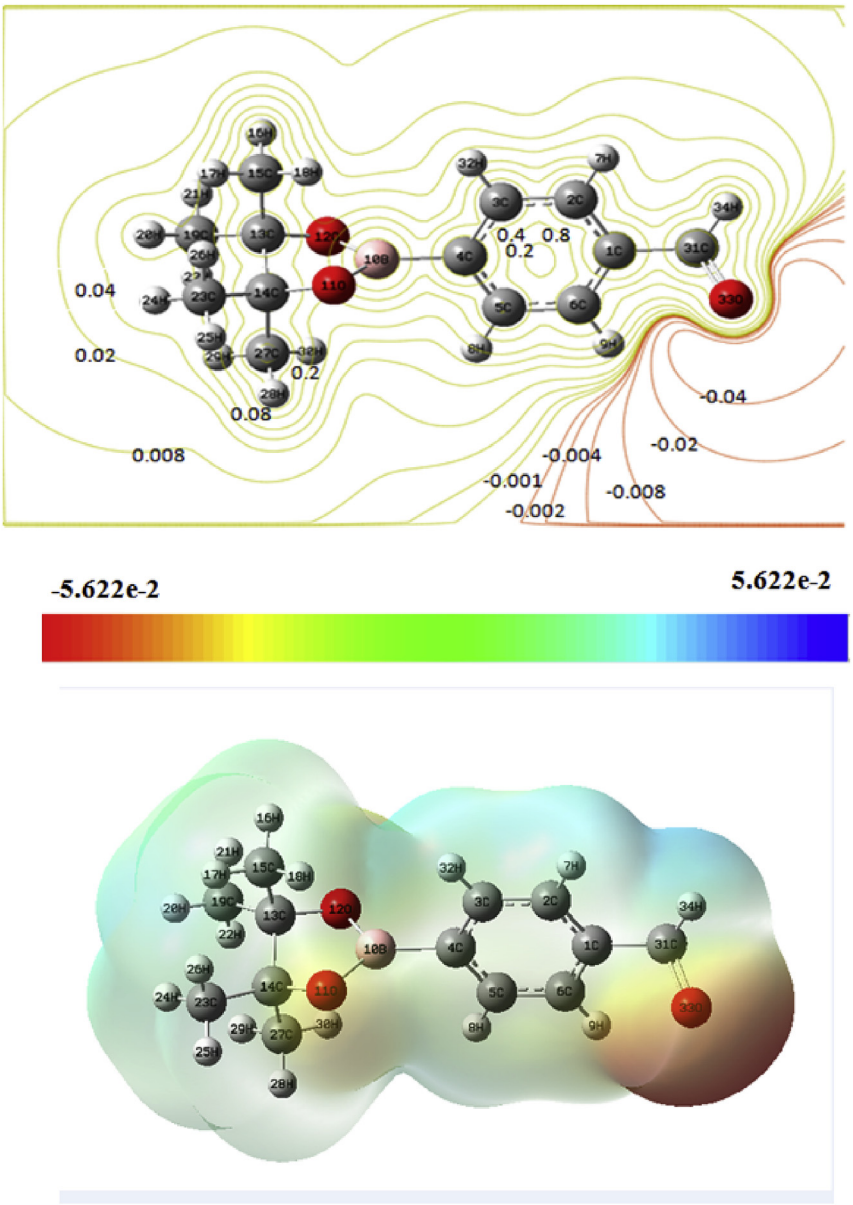

Fig. 12. Molecular electrostatic potential 3D and 2D contour map for 4-Formyl phenyl boronic acid pinacol ester.

Table 8
Comparison of Mulliken charges of 4-Formyl Phenyl Boronic Acid Pinacol Ester.

Atoms	4-Formyl Phenyl Boronic Acid Pinacol Ester	9H-Carbazole-9-(4-phenyl) boronic acid pinacol ester
C1	0.776	0.112
C2	−0.977	−0.064
C3	0.018	−0.119
C4	−0.274	−0.179
C5	−0.007	−0.119
C6	−0.128	−0.064
H7	0.125	0.113
H8	0.150	0.102
H9	0.150	0.113
B10	0.761	0.516
O11	−0.014	−0.335
O12	−0.026	−0.335
C13	−0.246	−0.017
C14	−0.223	−0.017
C15	-0.34	−0.243
H16	0.167	0.114
H17	0.147	0.107
H18	0.165	0.121
C19	−0.593	−0.232
H20	0.150	0.106
H21	0.160	0.117
H22	0.168	0.117
C23	−0.594	−0.232
H24	0.150	0.117
H25	0.160	0.106
H26	0.168	0.117
C27	−0.339	–
H28	0.167	–
H29	0.147	–
H30	0.165	–
C31	−0.124	–
H32	0.149	–
O33	−0.256	–
H34	0.099	–

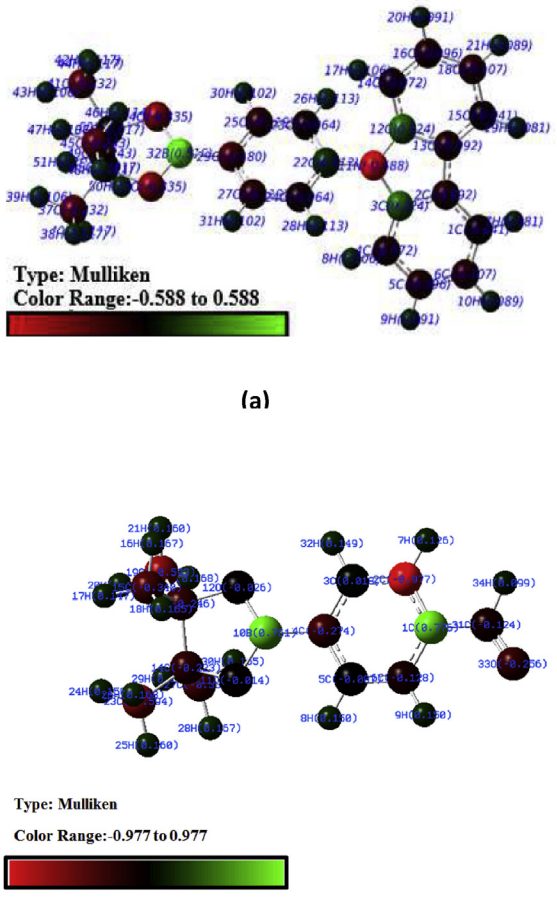

molecular properties such as the size, shape and regions [66,67]. It is a calculation technique frequently used to work out the nucleo- and electrophilic attacks in molecules.

At this visual presentation of chemical activity, the negative (red) regions of MEP are related to electrophilic reactivity and electron-donating reaction while the positive (blue) regions are pertinent to nucleophilic reactivity and electron-accepting reaction. MEP studies were performed using the B3LYP/6-311 + G(d,p) basis set and are presented in Fig. 12. All colors in this range from red to blue were used. Different colors on the MEP surface map show different values of electrostatic potential. The potential increases from red to blue. The regions with a negative potential were concentrated on O33 atom whereas the regions with a positive potential were concentrated around H atoms.

7.5. Mulliken atomic charges

Mulliken atomic charges of the molecule are listed in Table 8 and the charge distribution is illustrated in Fig. 13. Reactive atomic charges have a remarkable role within the molecular systems in terms of applying the quantum mechanical calculations. In the present study, Mulliken charges of similar molecules were calculated through different basis sets and the results were interpreted and compared with each other. While the charge distribution of 9-CPBAPE was calculated by the B3LYP/6-311G (d,p) basis set, Mulliken atomic charges of 4FPBAPE was calculated in this study by the DFT/B3LYP method and 6-311 + G(d,p) basis set.

The electron density of the phenyl ring in COH group led to a new distribution in terms of the results. While C1 carbon atom of the phenyl ring has a positive charge of 0.776 e in this study, C22 carbon atom of the 9-CPBAPE phenyl ring has a positive charge of 0.112 e. The same result is observed in the other atoms of the ring, which means that COH group is attached to the phenyl ring of 4FPBAPE molecule while carbazole molecule is attached to that of 9-CPBAPE.

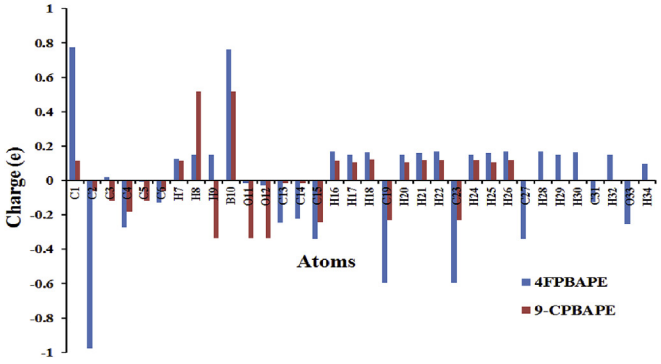

Fig. 13. The Mulliken charge distribution for 4-Formyl phenyl boronic acid pinacol ester and *9H*-Carbazole-9-(4-phenyl) boronic acid pinacol ester molecule.

7.6. Thermodynamic properties

Heat capacity at constant pressure (C), entropy (S), and enthalpy

Table 9
Thermodynamic properties of 4-Formyl Phenyl Boronic Acid Pinacol Ester at different temperatures.

Temperature (K)	Capacity (calmol^{-1} K^{-1})	Entropy(calmol^{-1} K^{-1})	Enthalpy(kcalmol^{-1})
100	24.956	81.713	1.666
150	35.403	94.643	3.279
200	45.188	106.748	5.394
250	54.888	118.315	7.995
298.15	64.27	129.135	10.960
300	64.629	129.546	11.082
350	74.187	140.537	14.653
400	83.288	151.309	18.692
450	91.746	161.849	23.171
500	99.486	172.131	28.053
550	106.517	182.138	33.306
600	112.886	191.857	38.893
650	118.661	201.283	44.783
700	123.91	210.419	50.949

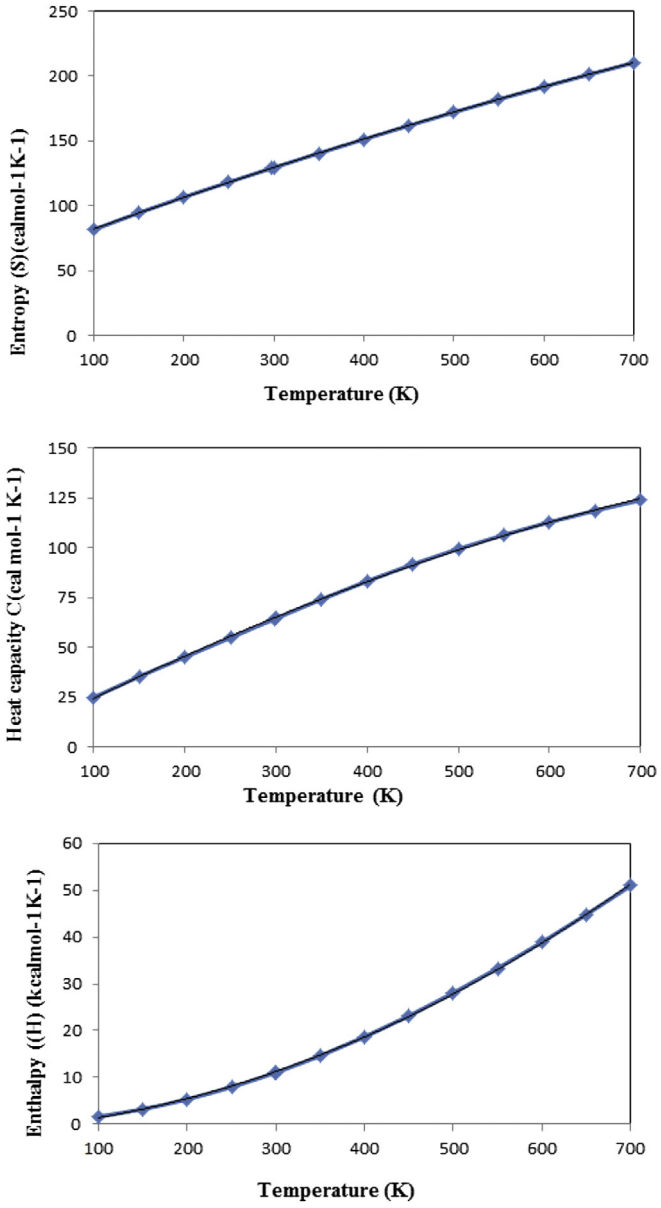

Fig. 14. Corelation graphics of enthalpy, entropy and heat capacity for 4-Formyl phenyl boronic acid pinacol ester molecule.

parameters (ΔH) were obtained for 4FPBAPE. So as to see the change in thermodynamic functions, temperature was scaled up from 100 K to 700 K (see Table 9). It was observed that thermodynamic functions increased with the rise of temperature due to the increment of molecular vibrational intensities depending on temperature increase [68]. Correlation graphs of these are shown in Fig. 14. Changes in C, S, and ΔH were fitted with the formulae below and the corresponding fitting factors (R^2) for these thermodynamic properties were found as 0.999, 1.000 and 0.999, respectively. The calculated thermo dynamical parameters of 4-Formyl Phenyl Boronic Acid Pinacol Ester at 298.15 K for all forms are tabulated in Table 10.

Corresponding fitting equations.

$$C = 0.657 + 0.244T - 1 \times 10^{-4}T^2 \left(R^2 = 0.999\right) \quad (1)$$

Table 10
The calculated thermo dynamical parameters of 4-Formyl Phenyl Boronic Acid Pinacol Ester at 298.15 K for all forms.

Symmetry group	C1
SCF energy(a.u.)	−756.472
Zero point vibrational energy(kcalmol^{-1})	175.847
Rotational constants(GHz)	1.28683
	0.20384
	0.19053
Specific heat, Cv(calmol^{-1}K^{-1})	64.270
Entropy, S(calmol^{-1}K^{-1})	129.135

Table 11
The dipole moments, polarizability (a.u.), average polarizability (x10^{-24} esu), anisotropy of the polarizability (x10^{-24} esu), and first hyperpolarizability (x10^{-33} esu) of 4-Formyl Phenyl Boronic Acid Pinacol Ester.

μ_x	−5.662	β_{xxx}	2684.885
μ_y	1.557	β_{xxy}	248.692
μ_z	−0.212	β_{xyy}	194.644
μ_0	5.876	β_{yyy}	707.568
α_{xx}	36.641	β_{xxz}	−171.421
α_{xy}	−0.439	β_{xyz}	−98.167
α_{yy}	24.623	β_{yyz}	−107.041
α_{xz}	−0.536	β_{xzz}	−419.477
α_{yz}	−1.054	β_{yzz}	142.039
α_{zz}	18.176	β_{zzz}	−39.318
α_{total}	26.480	β_x	2460.051
$\Delta\alpha$	65.508	β_y	1098.300
		β_z	−317.781
		β	2712.766

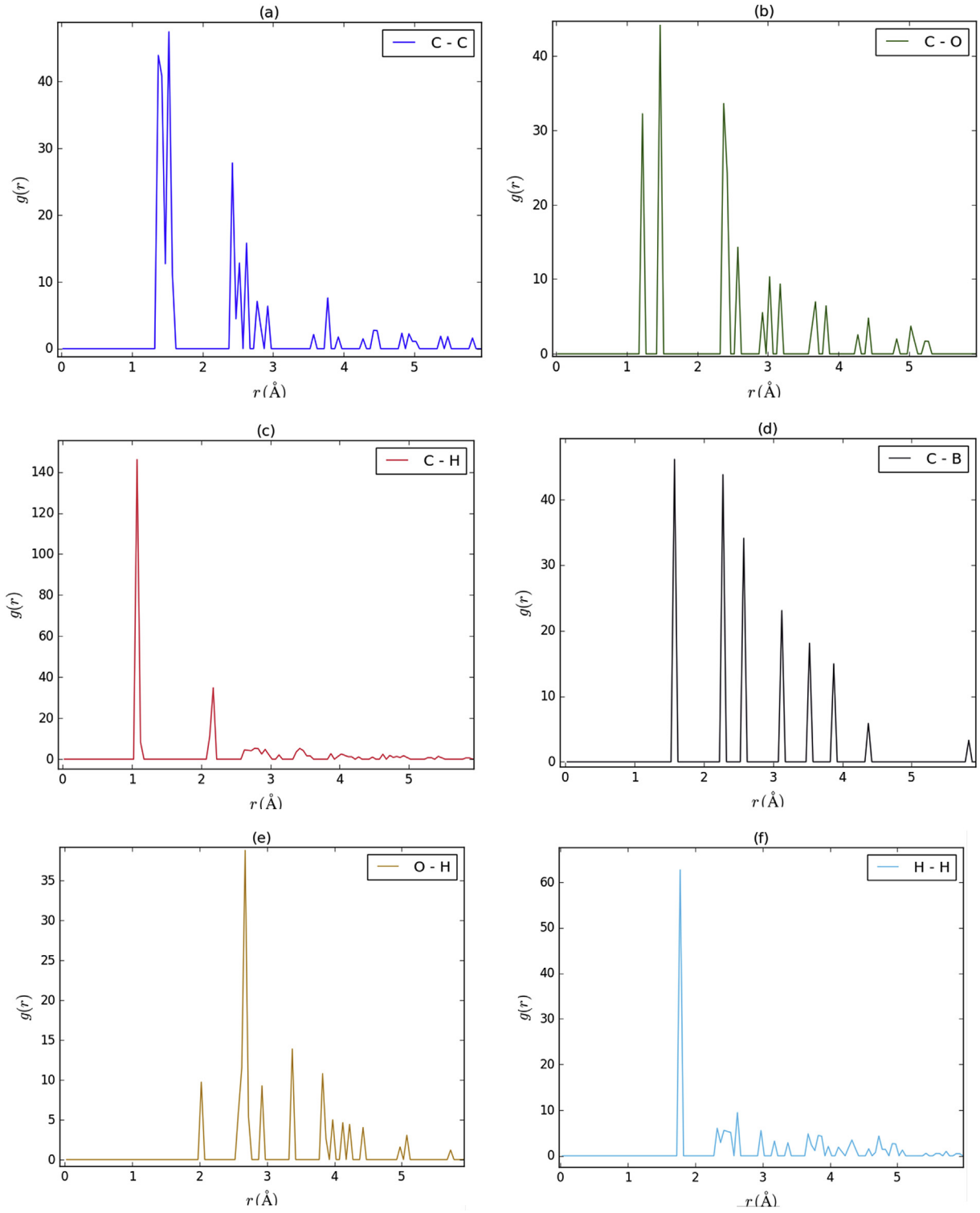

Figure 15. Radial distribution functions (RDFs) for carbon-carbon (C–C), carbon-oxygen (C–O), carbon-hydrogen (C–H), carbon-boron (C–B), oxygen-hydrogen (O–H) and hydrogen-hydrogen (H–H) atoms.

$$S = 56.7 + 0.256T - 6 \times 10^{-5}T^2 \left(R^2 = 1.000\right) \quad (2)$$

$$\Delta H = -0.937 + 0.015T + 8 \times 10^{-5}T^2 \left(R^2 = 0.999\right) \quad (3)$$

8. Nonlinear optical properties and dipole moment

Nonlinear optical properties, dipole moment, molecular polarizability, mean polarizability (α), anisotropy of polarizability ($\Delta\alpha$) and molecular hyperpolarizability (β) were calculated. The molecular polarizability and hyperpolarizability tensors were provided

via a Gaussian output file and its atomic units (a.u.) were converted to electronic units (esu) (1 a.u. = 0.1482 × 10^{-}24 esu for α; 1 a.u. = 8.6393 × 10^{-}33 esu for β). The values α, $\Delta\alpha$, and β were calculated using the equations below.

$$\alpha_{top} = \frac{1}{3}\left(\alpha_{xx} + \alpha_{yy} + \alpha_{zz}\right) \tag{4}$$

$$\Delta\alpha = \frac{1}{\sqrt{2}}\left[\left(\alpha_{xx} - \alpha_{yy}\right)^2 + \left(\alpha_{yy} - \alpha_{zz}\right)^2 + \left(\alpha_{zz} - \alpha_{xx}\right)^2 + 6\alpha_{xz}^2 + 6\alpha_{xy}^2 + 6\alpha_{yz}^2\right]^{\frac{1}{2}} \tag{5}$$

$$\langle\beta\rangle = \left[\left(\beta_{xxx} + \beta_{xyy} + \beta_{xzz}\right)^2 + \left(\beta_{yyy} + \beta_{yzz} + \beta_{yxx}\right)^2 + \left(\beta_{zzz} + \beta_{zxx} + \beta_{zyy}\right)^2\right]^{\frac{1}{2}} \tag{6}$$

The electronic dipole moment for 4FPBAPE molecule defined above and the total $\mu_i (i = x, y, z)$ ve μ_{tot} parameters are listed in Table 11. The total dipole moment was computed using the equation below.

$$\mu_{tot} = \left(\mu_x^2 + \mu_y^2 + \mu_z^2\right)^{\frac{1}{2}} \tag{7}$$

The dipole moment, polarizability and hyperpolarizability need to show higher values in order for the nonlinear optic properties to be more active. The 4-FPBAPE molecule exhibits a homogenous charge distribution. It, therefore, does not have a large dipole moment. The dipole moment was calculated as 5.8765 Debye. The highest dipole moment was observed in the μx (3.0637 Debye) compound and the lowest in the μz (0.9252 Debye) compound. The magnitude of molecular hyperpolarizability is a significant factor for the NLO systems. This value was calculated as 3675.1423 x 10^{-33} esu with the B3LYP/cc-vdpz method. The polarizability and anisotropy of polarizability for 4-FPBAPE were found respectively as 17.3242 x 10^{-24} esu and 56.3182 x 10^{-24} esu. The values of NLO-based hyperpolarizability, polarizability and anisotropy of polarizability for the studied molecule were observably larger than the normal values (the common values of urea).

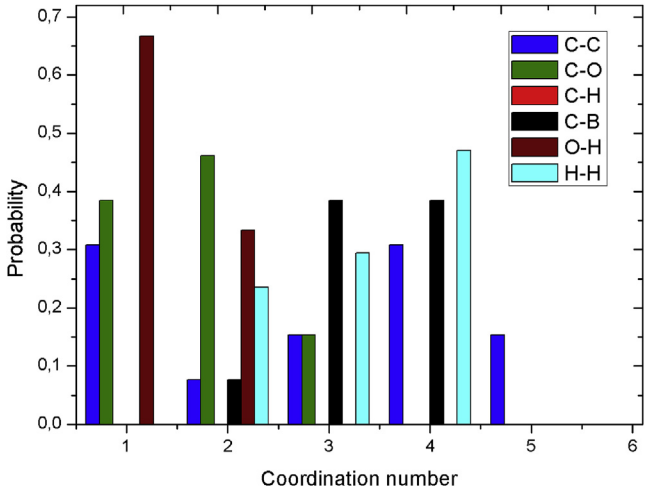

Fig. 16. Probability distributions of carbon-carbon (C–C), carbon-oxygen (C–O), carbon-hydrogen (C–H), carbon-boron (C–B), oxygen-hydrogen (O–H) and hydrogen-hydrogen (H–H) atoms depending on coordination number.

9. Radial distribution function and probablity density

Fig. 15 shows the radial distribution functions (RDFs) analysis for carbon-carbon (C–C), carbon-oxygen (C–O), carbon-hydrogen (C–H), carbon-boron (C–B), oxygen-hydrogen (O–H) and hydrogen-hydrogen (H–H) interactions of 4FPBAPE molecule. The RDFs is calculated for each atomic pairs of optimized 4FPBAPE molecule. One can see that C–H has a narrower and higher distribution. Moreover, there is a slight difference between C–C and C–O atoms. For C atoms, C–O is slightly shorter than C–C and C–B interactions; for H, O–H is shorter than C–H. For all of the combinations, C–H has stronger interactions than the other ones. To study the influence of interactions of the atoms in the molecule, we also performed the probability distribution depending on the coordination number (Fig. 16). The coordination number of C–C, C–O and O–H interactions significantly decrease while H–H hydrogen bonding interaction becomes weak due to lower cohesive energy between H–H interactions.

10. Conclusion

4FPBAPE molecule have been investigated via experimental and theoretical techniques. The results showed that the structure with minimum total energy of the 4FPBAPE is the A_1 form. The structural, electronic and spectroscopic properties have been researched using FT-IR, dispersive Raman, UV–Vis, ^{1}H and ^{13}C NMR techniques and DFT calculations. Radial distribution functions (RDF) and probability density depending on coordination number were also investigated to gain an insight behavior of between dimer interactions. Scaling factor (0.9684) was used and found that the observed and scale wave number values are almost the same. The thermodynamic properties are found to be increasing with the temperature increase. The calculated energy values for CAM-B3LYP functional are found to be more compatible with experimental results. We hope that the results will shed light on the study of material science and health practices.

References

[1] N.A. Petasis, Aust. J. Chem. 60 (2007) 795–798.
[2] P.C. Trippier, C. McGuigan, Med. Chem. Commun. 1 (2010) 183–198.
[3] D.G. Hall, Medicine and Materials, Wiley-VCH, Weinheim, 2011.
[4] Archana Kumar, Tania Ng, Sushant Malhotra, Jason Gruenhagen, Larry Wigman, J. Liq. Chromatogr. Relat. Technol. 37 (2014) 1985–1998.
[5] W. Yang, X. Gao, B. Wang, Med. Res. Rev. 23 (2003) 346–368.
[6] J. Zhang, P.L. Yang, N.S. Gray, Cancer 9 (2009) 28–39.
[7] C. Tsatsanis, D.A. Spandidos, Int. J. Mol. Med. 5 (2000) 583–590.
[8] N.M. Giles, G.I. Giles, C. Jacob, Biochem. Biophys. Res. Commun. 300 (2003) 1–4.
[9] C.J. Watson, P.A. Kreuzaler, J. Mammary Gland. Biol. Neoplasia 14 (2009) 171–179.
[10] E. Tsilikounas, C.A. Kettner, W.W. Bachovchin, Biochemistry 31 (1992) 12839–12846.
[11] T. Asano, H. Nakamura, Y. Uehara, Y. Yamamoto, ChemBioChem 5 (2004) 483–490.
[12] D. Chen, M. Frezza, S. Schmitt, J. Kanwar, Q.P. Dou, Curr. Cancer Drug Targets 11 (2011) 239–253.
[13] Soloway, A.H. Tjarks, W. Barnum, B. A. Rong, F.-G. Barth, R. F. Codogni, I. M., Wilson, J. G. 1998, 98, 1515–1562.
[14] M.S. Petersen, C.C. Petersen, R. Agger, M. Sutmuller, M.R. Jensen, P.G. Sorenser, M.W. Mortensen, T. Hansen, T. Bjornholm, H.J. Gundersen, et al., Anticancer Res. 28 (2008) 571–576.
[15] A.H. Soloway, R.G. Fairchild, Sci. Am. 262 (1990) 100.
[16] X. Chen, G. Liang, D. Whitmire, J.P. Bowen, J. Phys.Org. Chem. 11 (1988) 378–386.
[17] W. Tjarks, A.K.M. Anisuzzaman, L. Liu, S.H. Soloway, R.F. Barth, D.J. Perkins, D.M. Adams, J. Med. Chem. 35 (1992) 16228–17861.
[18] Y. Yamamoto, Pure Appl. Chem. 63 (1991) 423–426.
[19] F. Alam, A.H. Soloway, R.F. Barth, N. Mafune, D.M. Adam, W.H. Knoth, J. Med. Chem. 32 (1989) 2326–2330.
[20] M.K. Cyranski, A. Jezierska, P. Klimentowska, J.J. Panek, A. Sporzynski, J. Phys.Org. Chem. 21 (2008) 472–482.
[21] P.N. Horton, M.B. Hursthouse, M.A. Becket, M.P.R. Hankey, Acta Cryst. E60

(2004) o2204–o2206.
[22] M.R. Shimpi, N.S. Lekshmi, V.R. Pedireddi, Cryst. Growth Des. 7 (10) (2007) 1958–1963.
[23] P.R. Cuamatzi, H. Tlahuext, H. Hopfl., 2009, E65, o44–o45.
[24] D.C. Bradley, I.S. Harding, A.D. Keefe, M. Motevalli, D.H. Zheng, J. Chem. Soc. Dalton Trans. (1996) 3931–3936.
[25] J.A. Faniran, H.F. Shurvell, Can. J. Chem. 46 (1968) 2089.
[26] Y. Erdogdu, M.T. Gulluoglu, M. Kurt, J. Raman Spectrosc. 40 (2009) 1615–1623.
[27] M. Kurt, J. Mol. Struct. 874 (2008) 159–169.
[28] M. Kurt, J. Raman Spectrosc. 40 (2009) 67–75.
[29] M. Kurt, T.R. Sertbakan, M. Ozduran, M. Karabacak, J. Mol. Struct. 921 (2009) 178–187.
[30] M. Kurt, T.R. Sertbakan, M. Ozduran, Spectrochim. Acta Part A Mol. Biomol. Spectrosc. 70 (3) (2008) 664–673.
[31] S. Ayyappan, N. Sundaraganesan, M. Kurt, T.R. Sertbakan, M. Ozduran, J. Raman Spectrosc. 41 (2010) 1379–1387.
[32] O. Alver, Chimie 14 (5) (2011) 446–455.
[33] O. Alver, C. Parlak, Vib. Spectrosc. 54 (2010) 1–9.
[34] M. Karabacak, E. Kose, A. Atac, M.A. Cipiloglu, M. Kurt, Spectrochim. Acta Part A 97 (2012) 892–908.
[35] M. Karabacak, L. Sinha, O. Prasad, A.M. Asiri, M. Cinar, Spectrochim. Acta Part A 70 (2013) 753–766.
[36] U. Rani, M. Karabacak, O. Tanrıverdi, M. Kurt, N. Sundaraganesan, Spectrochim. Acta Part A 92 (2012) 67–77.
[37] M. Karabacak, E. Köse, A. Atac, A.M. Asiri, M. Kurt, J. Mol. Struct. 1058 (2014) 79–96.
[38] N. Piergies, E. Proniewicz, Y. Ozaki, Y. Kim, L.M. Proniewicz, J. Phys. Chem. A 117 (2013) 5693–5705.
[39] N. Piergies, E. Proniewicz, A. Kudelski, A. Rydzewska, Y. Kim, M. Andrzejak, L.M. Proniewicz, J. Phys. Chem. A 116 (2012) 10004–10014.
[40] P. Hohenberg, W. Kohn, Phys. Rev. 136 (1964) B864–B871.
[41] A.D. Becke, J. Chem. Phys. 98 (1993) 5648–5652.
[42] C. Lee, W. Yang, R.G. Parr, Phys. Rev. B 37 (1988) 785–789.
[43] M.J. Frisch et al., GAUSSIAN 09, Revision A.1, Gaussian Inc., Wallingford, CT.
[44] M.H. Jamroz, Mol. Biomol. Spectrosc. 114 (2013) 220–230.
[45] G. Keresztury, S. Holly, J. Varga, G. Besenyei, A.Y. Wang, J.R. Durig, Spectrochim. Acta 49 (1993) 2007–2017.
[46] G. Keresztury, J.M. Chalmers, P.R. Griffith (Eds.), 1, John Wiley&Sons Ltd., New York, 2002.
[47] R. Ditchfield, J. Chem. Phys. 56 (1972) 5688–5691.
[48] K. Wolinski, J.F. Hinton, P. Pulay, J. Am. Chem. Soc. 112 (1990) 8251–8260.
[49] N.M. O'Boyle, A.L. Tenderholt, K.M. Langner, J.Compd. Chem. 29 (2008) 839–845.
[50] R.M. Silverstein, F.X. Webster, D.J. Kiemle, John Wiley & Sons, 2005.
[51] G. Socrates, Infrared and Raman Characteristic Group Frequencies: Tables and Charts, John Wiley & Sons Ltd., West Sussex, England, 2001.
[52] G. Varsanyi, Halsted Press, 1974.
[53] V. Krishnakumar, R.J. Xavier, Indian J. Pure Appl. Phys. 41 (2003) 95–98.
[54] K. Furic, V. Mohacek, M. Bonifacic, I. Stefanic, J. Mol. Struct. 267 (1992) 39–44.
[55] N.P. Singh, R.A. Yadav, Indian J. Phys. B75 (4) (2001) 347–352.
[56] P.B. Nagabalasubramanian, M. Karabacak, S. Periandy, J. Mol. Struct. 1017 (2012) 1–13.
[57] N. Subramania, N. Sundaraganesan, J. Jayabharathi, Spectrochim. Acta A 76 (2010) 259–269.
[58] A. Coruh, F. Yilmaz, B. Sengez, M. Kurt, M. Cinar, M. Karabacak, Struct. Chem. 22 (2011) 45–56.
[59] H.O. Kalinowski, S. Berger, S. Braun, Carbon-13NMR Spectroscopy, John Wiley & Sons, Chichester, 1988.
[60] K. Pihlaja, E. Kleinpeter (Eds.), VCH Publishers, Deerfield Beach, 1994.
[61] K. Fukui, Science 218 (1982) 747–754.
[62] M. Arivazhagan, D. Anitha Rexalin, Spectrochim. Acta A 96 (2012) 668–676.
[63] T. Hughbanks, R. Hoffmann, J. Am. Chem. Soc. 105 (1983) 3528–3537.
[64] J.G. Małecki, Polyhedron 29 (2010) 1973–1979.
[65] M. Chen, U.V. Waghmare, C.M. Friend, E. Kaxiras, J. Chem. Phys. 109 (1998) 6854–6860.
[66] J. Murray, K. Sen, 1 st edition, Elsevier, Amsterdam, 1996.
[67] E. Scrocco, J. Tomasi, Adv. Quantum Chem. 11 (1978) 115–193.
[68] J.B. Ott, J. Boerio-Goates, Academic Press, 2000.